Integral-direct coupled cluster calculations of frequency-dependent polarizabilities, transition probabilities and excited-state properties

Ove Christiansen, Asger Halkier, Henrik Koch, and Poul Jørgensen
Department of Chemistry, Århus University, DK-8000 Århus, Denmark

Trygve Helgaker
Department of Chemistry, University of Oslo, P.O. Box 1033 Blindern, N-0315 Norway

(Received 30 September 1997; accepted 11 November 1997)

An atomic integral-direct implementation of molecular linear-response properties and excited-state one-electron properties is presented for the coupled cluster models CCS, CC2, and CCSD. Sample calculations are presented for the polarizability of N_2 and for excited-state one-electron properties and transition-properties of furan. © *1998 American Institute of Physics.*
[S0021-9606(98)01607-9]

I. INTRODUCTION

The coupled cluster model constitutes the most successful electronic-structure model in modern quantum chemistry for describing dynamical correlation effects for general molecular properties of systems dominated by a single electronic configuration. Its popularity has gradually increased since the first implementation of the coupled cluster singles and doubles (CCSD) model.[1] The advantages of the coupled cluster model for the calculation of ground-state energies, geometries and other frequency-independent properties are now well-known and well-documented and have been reviewed several places in the literature.[2,3]

In a recent series of articles, we have presented an atomic integral-direct coupled cluster algorithm,[4–8] which has made it possible to employ larger and more complete one-electron basis sets, thus allowing sequences of calculations to be carried out where the basis set is systematically improved toward giving the basis set limit results. We have further introduced the hierarchy of coupled cluster models CCS, CC2, CCSD, and CC3,[9–12] where molecular properties can be calculated with increased accuracy in the N-electron space at the expense of increasing complexity in the calculation. Initial benchmark calculations on electronic excitation energies have been encouraging.[7,13,14]

In this work we describe an atomic integral-direct implementation for CCS, CC2 and CCSD calculations of molecular properties from the linear-response function and its residues and also from the double residue of the quadratic response function. This allows the calculation of frequency-dependent polarizabilities and one-photon transition-matrix elements. It also makes possible the calculation of excited state one-electron properties as the electric multipole moments and one-photon transition-matrix elements between excited states. Previous implementations of the calculation of second-order ground-state properties has been described for CCSD[15–18] using various expressions, and also for CC2.[19] The implemented equations in this work are based on our recent derivation of coupled cluster frequency-dependent response functions[20] and use response function expressions that are generalized compared to the ones in Refs. 15, 21. Excited-state properties have been implemented before in another context.[22]

The twin adoption of a hierarchy of coupled cluster models and hierarchies of correlation-consistent basis sets is important for monitoring the accuracy of calculated excitation energies. Oscillator strengths and excited-state properties are important for the characterization of the excited electronic states and give information that is useful for the qualitative assignment of the excited states, for example in terms of valence and Rydberg states. We report sample calculations on furan to illustrate these points. In a subsequent publication, these results will be used to perform a more detailed comparison with the theoretical and experimental electronic spectrum of furan. To demonstrate the applicability of the implementation of calculation of second-order molecular properties, we report calculations of the frequency-dependent polarizability of the nitrogen molecule, carrying out a basis-set investigation and comparing with experimental frequency-dependent polarizabilities and results derived from the refractive index.

This paper is organized as follows. In the next section, we present the theory and describe our atomic integral-direct implementation. In Section III, we present the application to the polarizability of N_2, and in Section IV we describe the results for the transition properties and excited-state properties of furan. Finally in Section V, we give our concluding remarks.

II. THEORY

A. Response theory for exact states

Consider a molecular system described by a time-independent Hamiltonian H_o. We now apply a time-dependent perturbation V^t to the system. The time-evolution of the system is governed by the time-dependent Schrödinger equation

$$H|\overline{O}\rangle = i\partial/\partial t|\overline{O}\rangle, \tag{1}$$

where we write the Hamiltonian as a sum of the unperturbed molecular Hamiltonian H_o and the time dependent perturbation V^t

$$H = H_o + V^t. \tag{2}$$

We consider perturbations of the form

$$V^t = \sum_y \epsilon_y(\omega_y) Y \exp(-i\omega_y t). \tag{3}$$

We require that $\epsilon_y(\omega_y) = \epsilon_y(-\omega_y)^*$ and that the operators Y are Hermitian, so that V^t is Hermitian. The observables of the system evolve in time according to the evolution of $|\overline{O}\rangle$. We now expand the time-dependent expectation value $\langle \overline{O}|X|\overline{O}\rangle$ of the operator X in orders of the perturbation V^t:

$$\begin{aligned}\langle \overline{O}|X|\overline{O}\rangle = \langle 0|X|0\rangle + \sum_y \epsilon_y(\omega_y)\langle\langle X,Y\rangle\rangle_{\omega_y} \exp(-i\omega_y t) \\ + \sum_{y,z} \epsilon_y(\omega_y)\epsilon_z(\omega_z)\langle\langle X,Y,Z\rangle\rangle_{\omega_y,\omega_z} \\ \times \exp(-i(\omega_y+\omega_z)t) + O(3),\end{aligned} \tag{4}$$

where $O(3)$ indicates higher-order terms. The first term $\langle 0|X|0\rangle$ is the expectation value in the absence of V^t where the unperturbed wave function is denoted $|0\rangle$. The expansion coefficient $\langle\langle X,Y\rangle\rangle_{\omega_y}$ is the linear-response function controlling the linear response of the expectation value $\langle \overline{O}|X|\overline{O}\rangle$ to the perturbation Y oscillating with frequency ω_y. The expansion coefficient $\langle\langle X,Y,Z\rangle\rangle_{\omega_y,\omega_z}$ is the quadratic response function, controlling the quadratic response of the expectation value $\langle \overline{O}|X|\overline{O}\rangle$ to the perturbations Y and Z oscillating with frequencies ω_y and ω_z respectively.

For exact states, the linear-response function can be written in terms of the unperturbed eigenstates $\{|O\rangle,|k\rangle\}$ of H_o as

$$\begin{aligned}\langle\langle X,Y\rangle\rangle_{\omega_y} &= P(X(\omega_x),Y(\omega_y))\sum_k \frac{\langle 0|X|k\rangle\langle k|Y|0\rangle}{\omega_y-\omega_k} \\ &= \sum_k \left[\frac{\langle 0|X|k\rangle\langle k|Y|0\rangle}{\omega_y-\omega_k} - \frac{\langle 0|Y|k\rangle\langle k|X|0\rangle}{\omega_y+\omega_k}\right].\end{aligned} \tag{5}$$

Here $\omega_k = E_k - E_o$, where E_o is the ground-state energy and E_k is the energy of the excited-state k. The operator $P(X(\omega_x),Y(\omega_y))$ generates the two permutations of the operators and related frequencies $(X,\omega_x),(Y,\omega_y)$ where $\omega_x = -\omega_y$. Note that the exact linear-response functions satisfy the symmetry relation

$$\langle\langle X,Y\rangle\rangle_{\omega_y} = (\langle\langle X,Y\rangle\rangle_{-\omega_y})^*. \tag{6}$$

The linear-response function has poles at $\omega_y = \pm\omega_f$, where ω_f is the excitation energy for state f. The corresponding residue is

$$\lim_{\omega_y\to\omega_f} (\omega_y-\omega_f)\langle\langle X,Y\rangle\rangle_{\omega_y} = \langle 0|X|f\rangle\langle f|Y|0\rangle. \tag{7}$$

The residue $\omega_x = -\omega_y = \omega_f$ is obtained by permuting X and Y. The residue thus contains information on the transition strength between the ground-state 0 and the excited-state f

$$\begin{aligned}S^{of}_{XY} = \langle 0|X|f\rangle\langle f|Y|0\rangle = \frac{1}{2}(\langle 0|X|f\rangle\langle f|Y|\rangle + \langle 0|Y|f\rangle \\ \times\langle f|X|0\rangle).\end{aligned} \tag{8}$$

The linear-response function contains information on all one-photon processes and thus all frequency-dependent properties. The frequency-dependent polarizability is obtained by substituting dipole operators for X and Y. Static molecular properties are obtained by introducing the appropriate operators and setting $\omega_y = 0$. The oscillator-strength matrix for ground- to excited-state transitions is obtained as $\frac{2}{3}\omega_f S^{of}_{XY}$ with X and Y being the electric dipole operators. Note that the operators X and Y can be replaced by arbitrary Hermitian operators and are thus not restricted to dipole operators.

Adding the excitation energy to the total ground-state energy, we obtain the total energy of the excited state

$$E^f = E_o + \omega_f. \tag{9}$$

From this expression, we can determine excited-state first-order properties, applying an external field and differentiating with respect to the perturbation strength at zero frequency

$$\langle X\rangle^f = \frac{dE^f}{d\epsilon_x(0)}. \tag{10}$$

For an exact state the quadratic response function can be written as

$$\begin{aligned}\langle\langle X,Y,Z\rangle\rangle_{\omega_y,\omega_z} = -P(X(\omega_x),Y(\omega_y),Z(\omega_z)) \\ \times\sum_{j,k} \frac{\langle 0|X|j\rangle\langle j|\overline{Y}|k\rangle\langle k|Z|0\rangle}{(\omega_x+\omega_j)(\omega_z-\omega_k)},\end{aligned} \tag{11}$$

where $\omega_x = -\omega_y - \omega_z$ and

$$\overline{Y} = Y - \langle O|Y|O\rangle. \tag{12}$$

The first residue of the quadratic response function is related to the product of one- and two-photon transition-matrix elements. Two-photon transitions are not considered further here. We consider only the second residue

$$\begin{aligned}\lim_{\omega_y\to\omega_i}(\omega_y-\omega_f)\lim_{\omega_z\to-\omega_f}(\omega_z+\omega_f)\langle\langle X,Y,Z\rangle\rangle_{\omega_y,\omega_z} \\ = -\langle 0|Z|f\rangle\langle f|\overline{Y}|i\rangle\langle i|Y|0\rangle.\end{aligned} \tag{13}$$

For $f=i$, we determine first-order properties for the excited state that are equivalent to the ones obtained from using Eq. (10). For $f\neq i$, we obtain information on the transition-matrix elements between the excited states. Accordingly, we introduce the transition-strength matrix between the excited states as

$$S^{if}_{XY} = \langle i|X|f\rangle\langle f|Y|i\rangle = \frac{1}{2}(\langle i|X|f\rangle\langle f|Y|i\rangle + \langle i|Y|f\rangle\langle f|X|i\rangle). \tag{14}$$

To derive the expressions for the response functions, it is convenient to parametrize the wave function as

$$|\overline{O}\rangle = \exp(-iP)|\widetilde{O}\rangle, \tag{15}$$

where, in the unperturbed limit, $|\widetilde{O}\rangle$ becomes the unperturbed time-independent wave function $|O\rangle$ and the generalized phase P becomes the usual phase factor for stationary states. Inserting Eq. (15) into the time-dependent Schrödinger equation and projecting onto $|\widetilde{O}\rangle$ we determine the time-dependence of $\dot{P}$

$$Q = \dot{P} = \langle \widetilde{O}|(H - i\partial/\partial t)|\widetilde{O}\rangle. \tag{16}$$

We denote Q the time-dependent quasi-energy. The response equations and response functions can be determined as derivatives of the time average of this quasi-energy. This formulation is especially convenient for derivation of response functions for non-variational models such as the coupled cluster model.[20]

B. The coupled cluster models CCS, CC2, and CCSD

The ansatz for the time evolution of the coupled cluster wave function may be expressed as

$$|CC\rangle = \exp(-iP)\exp(T)|HF\rangle. \tag{17}$$

For later convenience we choose the reference state to be the Hartree-Fock state $|HF\rangle$, but it is not a restriction in the theory. The cluster operator T consists of one-, two-... up to n-electron cluster operators

$$T = T_1 + T_2 + \ldots . T_n, \tag{18}$$

where n is the number of electrons in the system. The i'th cluster operator can be written in terms of products of i'th order excitation operators τ_{μ_i} and time-dependent cluster amplitudes t_{μ_i},

$$T_i = \sum_{\mu_i} \tau_{\mu_i} t_{\mu_i}, \tag{19}$$

where the excitation operators commute

$$[\tau_{\mu_i}, \tau_{\nu_j}] = 0. \tag{20}$$

Insertion of Eq. (17) into the time-dependent Schrödinger equation Eq. (1) followed by transformation with $\exp(iP)\exp(-T)$ gives

$$\exp(-T)H\ \exp(T)|HF\rangle = \left(Q - \sum_{\mu_i} \tau_{\mu_i} \dot{t}_{\mu_i} \right)|HF\rangle. \tag{21}$$

We have here assumed that the reference state $|HF\rangle$ is fixed and thus time-independent, and that a left-projection manifold ($\langle \mu_i| = \langle HF|\tau_{\mu_i}{}^{\dagger}, i = 1,2,..,n$) satisfying bi-orthonormality condition

$$\langle \mu_i|\nu_j\rangle = \langle HF|\tau_{\mu_i}{}^{\dagger}\tau_{\nu_j}|HF\rangle = \delta_{ij}\delta_{\mu\nu} \tag{22}$$

can be constructed. Left-projection onto $\langle HF|$ and the manifold comprising singly, doubly, and up to n-tuple excitations yields the following equations for Q

$$Q = \langle HF|H\ \exp(T)|HF\rangle, \tag{23}$$

and the coupled cluster amplitudes

$$\langle \mu_i|\exp(-T)H\ \exp(T)|HF\rangle = -i\dot{t}_{\mu_i}. \tag{24}$$

In the time-independent limit, Eqs. (23)–(24) reduce to the usual coupled cluster energy

$$E_{CC} = \langle HF|H\ \exp(T)|HF\rangle, \tag{25}$$

and amplitude equations

$$e_{\mu_i} = \langle \mu_i|\exp(-T)H\ \exp(T)|HF\rangle = 0. \tag{26}$$

The parametrization in Eqs. (17)–(26) is an alternative representation of the FCI state. Approximate coupled cluster models is introduced by truncating the cluster expansion in Eq. (18). This determines the standard series of coupled cluster approximations: CCS, CCSD, CCSDT, ... where CCS is obtained with $T = T_1$, CCSD with $T = T_1 + T_2$ and so on. Other approximate coupled cluster models like CC2 and CC3 can be introduced by performing additional approximations in the cluster amplitude equations. To describe the relationship between CC2 and CCSD, we invoke a Møller-Plesset type of partitioning of the Hamiltonian

$$H = F + V^t + U, \tag{27}$$

where F is the Fock operator, V^t is the external perturbation in Eq. (3), and U is the fluctuation potential. We do not include V^t in F since the Hartree–Fock reference state and therefore also the Fock operator is fixed. It is convenient to introduce T_1-similarity transformed operators

$$\hat{O} = \exp(-T_1)O\ \exp(T_1). \tag{28}$$

Using Eqs. (23)–(24) for the coupled cluster expansion truncated after doubles excitations, we may determine the CCSD singles and doubles amplitudes from the non-linear equations

$$\langle \mu_1|F + V^t + [F + \hat{V}^t, T_1] + \hat{U} + [\hat{U}, T_2]|HF\rangle = -i\dot{t}_{\mu_1}, \tag{29}$$

$$\langle \mu_2|V^t + [F + \hat{V}^t, T_2] + \hat{U} + [\hat{U}, T_2] + [[\hat{U}, T_2], T_2]|HF\rangle = -i\dot{t}_{\mu_2}. \tag{30}$$

In a canonical basis, $\langle \mu_1|F|HF\rangle$ is zero.

In CC2, the singles equations remains identical to those of CCSD, whereas only the terms occurring in lowest non-vanishing order in U are retained in the doubles equations. In approximating the doubles equations, the singles amplitudes are treated as zero-order parameters. This is most conveniently achieved by taking $\hat{U}$ as an effective first-order Hamiltonian. The CC2 double-excitation amplitude equation then becomes[9]

$$\langle \mu_2|F + V^t + [F + \hat{V}^t, T_2] + \hat{U}|HF\rangle = -i\dot{t}_{\mu_2}, \tag{31}$$

The same equations are used for the quasi-energy and energy in CC2 and CCSD.

In CCS theory, only singles excitations are included in the cluster expansion. Accordingly, the CCS cluster amplitude equations become

$$\langle \mu_1|\exp(-T_1)H\ \exp(T_1)|HF\rangle = -i\dot{t}_{\mu_1}. \tag{32}$$

In the unperturbed time-independent case, Eq. (32) has the solution

$$T_1^{\mathrm{CCS}}=0 \tag{33}$$

due to the Brillouin theorem for the reference Hartree–Fock state. The unperturbed CCS ground-state energy therefore reduces to the Hartree–Fock energy

$$E_{\mathrm{CCS}}=\langle HF|H\exp(T_1^{\mathrm{CCS}})|HF\rangle=\langle HF|H|HF\rangle=E_{HF}. \tag{34}$$

This is probably the reason why the CCS model has been overlooked in the literature. It should be emphasized that, although the CCS ground-state energy is identical to the Hartree–Fock energy, its response properties are in general different from the Hartree–Fock response properties.

C. Coupled cluster linear response theory

In the previous section, the time-dependent amplitude equations and the time-dependent quasi-energy were identified for CCS, CC2, and CCSD. From this a coupled cluster quasienergy is constructed

$$L_{CC}=Q+\sum_{\mu_i}\overline{t}_{\mu_i}(e_{\mu_i}-i\partial t_{\mu_i}/\partial t). \tag{35}$$

The form of Q and e_{μ_i} for the different models is obtained from Eqs. (23), (29), (30), (31), (32). The parameters $\overline{t}_{\mu_i}$ are the Lagrangian multipliers. This is sufficient to determine the response functions as derivatives of the time-averaged quasienergy. We refer to Refs. 9,11,20 for the detailed derivation of these quantities. Here we shall instead summarize the results needed in this context for the CCS, CC2 and CCSD models.

The coupled cluster linear response function can be derived as

$$\langle\langle X,Y\rangle\rangle_{\omega_y}=\frac{1}{2}C^{\pm\omega}P(X(\omega_x),Y(\omega_y))\times\left[\eta^X t^Y(\omega_y)+\frac{1}{2}\mathbf{F}t^X(\omega_x)t^Y(\omega_y)\right]. \tag{36}$$

The operator $C^{\pm\omega}$ symmetrizes with respect to simultaneous complex conjugation and reversal of all signs of the frequencies to ensure that the symmetry relation in Eq. (6) is satisfied

$$C^{\pm\omega}f(\omega_x,\omega_y)=f(\omega_x,\omega_y)+(f(-\omega_x,-\omega_y))^*. \tag{37}$$

The first-order responses of the cluster amplitudes are determined from

$$(\mathbf{A}-\omega_y\mathbf{1})t^Y(\omega_y)+\xi^Y=0. \tag{38}$$

An alternative expression for the coupled cluster linear response function is

$$\langle\langle X,Y\rangle\rangle_{\omega_y}=\frac{1}{2}C^{\pm\omega}[\eta^X t^Y(\omega_y)+\overline{t^Y}(\omega_y)\xi^Y], \tag{39}$$

where $\overline{t^Y}(\omega_y)$ is the first-order Lagrange-multiplier response determined from

$$\overline{t^y}(\omega_y)(\mathbf{A}+\omega_y\mathbf{1})+\eta^Y+\mathbf{F}t^Y(\omega_y)=0. \tag{40}$$

Expressions for the vectors η^X and ξ^Y together with the coupled cluster Jacobian $\mathbf{A}$ and the $\mathbf{F}$ matrix are listed in Table I for the CCS, CC2 and CCSD models. In Table I we have used the notation

$$\langle\overline{t_i}|=\sum_{\mu_i}\overline{t}_{\mu_i}\langle\mu_i|, \tag{41}$$

where $\overline{t}$ are the zero-order Lagrange multipliers obtained from

$$\overline{t}\,\mathbf{A}+\eta=0. \tag{42}$$

The η-vectors are also listed in Table I. It is understood that t and $\overline{t}$ refers to zero-order (unperturbed) amplitudes and multipliers. It is advantageous to use the two forms of the linear response function Eqs. (36) and (39) under different circumstances. Equation (36) requires the solution of first-order amplitude response equations with respect to both X and Y, whereas Eq. (39) requires the solution of first-order amplitudes and first-order multiplier response equations with respect to Y. For evaluation of the complete polarizability tensor it is therefore advantageous to use Eq. (36) since the number of X and Y perturbations are the same. The use of Eq. (39) is advantageous when the number of X operators is larger than the number of Y operators. The most obvious example of the latter is the calculation of nuclear magnetic shielding tensors.[16]

A pole and residue analysis of the coupled cluster linear-response function determines expressions for excitation energies and transition strengths for ground- to excited-state transitions. Accordingly, excitation energies in coupled cluster response theory are found as the eigenvalues of the coupled cluster Jacobian $\mathbf{A}$

$$\mathbf{A}R^f=\omega_f R^f, \tag{43}$$

where R^f is a right eigenvector and ω_f is the associated excitation energy (eigenvalue). Since the coupled cluster Jacobian is not symmetric, the left and right eigenvectors are not simply each other's adjoints. The left eigenvectors L^f are determined from

$$L^f\mathbf{A}=L^f\omega_f. \tag{44}$$

The left and right eigenvectors can be chosen to satisfy the bi-orthonormal condition

$$L^fR^g=\delta_{fg}. \tag{45}$$

From the residue of the linear-response function the transition strength for ground- to excited-state transitions is obtained as

$$S_{XY}^{of}=\frac{1}{2}(T_{of}^X T_{fo}^Y+(T_{of}^Y T_{fo}^X)^*), \tag{46}$$

where from Eq. (36) we obtain

$$T_{fo}^Y=L^f\xi^Y, \tag{47}$$

$$T_{of}^Y=\eta^Y R^f+\mathbf{F}t^Y(\omega_f)R^f. \tag{48}$$

From Eq. (39), we obtain an alternative form of T_{of}^Y

TABLE I. Response vector and matrices for CCS, CC2 and CCSD.[a,b]

Name	Model		
η	CCS	$\eta_{\nu_1}=\langle HF\vert[\hat{H}_o,\tau_{\nu_1}]\vert HF\rangle$[b]	
	CC2 & CCSD	$\eta_{\nu_1}=\langle HF\vert[\hat{H}_o,\tau_{\nu_1}]\vert HF\rangle$	$\eta_{\nu_2}=\langle HF\vert[H_o,\tau_{\nu_2}]\vert HF\rangle$
η^Y	CCS	$\eta^Y_{\nu_1}=\langle HF\vert[\hat{Y},\tau_{\nu_1}]\vert HF\rangle$	
	CC2 & CCSD	$\eta^Y_{\nu_1}=(\langle HF\vert+\langle \overline{t_1}\vert)[\hat{Y},\tau_{\nu_1}]\vert HF\rangle$ $+\langle \overline{t_2}\vert[\hat{Y}+[\hat{Y},T_2],\tau_{\nu_1}]\vert HF\rangle$	$\eta^Y_{\nu_2}=(\langle \overline{t_1}\vert+\langle \overline{t_2}\vert)[Y,\tau_{\nu_2}]\vert HF\rangle$
ξ^Y	CCS	$\xi^Y_{\mu_1}=\langle\mu_1\vert\hat{Y}\vert HF\rangle$	
	CC2 & CCSD	$\xi^Y_{\mu_1}=\langle\mu_1\vert\hat{Y}+[\hat{Y},T_2]\vert HF\rangle$	
		$\xi^Y_{\mu_2}=\langle\mu_2\vert\hat{Y}+[\hat{Y},T_2]\vert HF\rangle$	
A	CCS	$A_{\mu_1\nu_1}=\langle\mu_1\vert[\hat{H}_o,\tau_{\nu_1}]\vert HF\rangle$	
	CC2	$A_{\mu_1\nu_1}=\langle\mu_1\vert[\hat{H}_o+[\hat{H}_o,T_2],\tau_{\nu_1}]\vert HF\rangle$	$A_{\mu_1\nu_2}=\langle\mu_1\vert[\hat{H}_o,\tau_{\nu_2}]\vert HF\rangle$
		$A_{\mu_2\nu_1}=\langle\mu_2\vert[\hat{H}_o,\tau_{\nu_1}]\vert HF\rangle$	$A_{\mu_2\nu_2}=\delta_{\mu\nu}\omega_{\mu_2}$
	CCSD	$A_{\mu_1\nu_1}=\langle\mu_1\vert[\hat{H}_o+[\hat{H}_o,T_2],\tau_{\nu_1}]\vert HF\rangle$	$A_{\mu_1\nu_2}=\langle\mu_1\vert[\hat{H}_o,\tau_{\nu_2}]\vert HF\rangle$
		$A_{\mu_2\nu_1}=\langle\mu_2\vert[\hat{H}_o+[\hat{H}_o,T_2],\tau_{\nu_1}]\vert HF\rangle$	$A_{\mu_2\nu_2}=\langle\mu_2\vert[\hat{H}_o+[\hat{H}_o,T_2],\tau_{\nu_2}]\vert HF\rangle$
F	CCS	$F_{\mu_1\nu_1}=\langle HF\vert[[\hat{H}_o,\tau_{\mu_1}],\tau_{\nu_1}]\vert HF\rangle$	
	CC2	$F_{\mu_1\nu_1}=(\langle HF\vert+\langle \overline{t_1}\vert+\langle \overline{t_2}\vert)[[\hat{H}_o,\tau_{\mu_1}],\tau_{\nu_1}]\vert HF\rangle$	$F_{\mu_1\nu_2}=\langle \overline{t_1}\vert[[H_o,\tau_{\mu_1}],\tau_{\nu_2}]\vert HF\rangle$
		$F_{\mu_2\nu_1}=\langle \overline{t_1}\vert[[H_o,\tau_{\mu_2}],\tau_{\nu_1}]\vert HF\rangle$	$F_{\mu_2\nu_2}=0$
	CCSD	$F_{\mu_1\nu_1}=(\langle HF\vert+\langle \overline{t_1}\vert+\langle \overline{t_2}\vert)[[\hat{H}_o,\tau_{\mu_1}],\tau_{\nu_1}]\vert HF\rangle$ $+\langle \overline{t_2}\vert[[[\hat{H}_o,\tau_{\mu_1}],\tau_{\nu_1}],T_2]\vert HF\rangle$	$F_{\mu_1\nu_2}=(\langle \overline{t_1}\vert+\langle \overline{t_2}\vert)[[H_o,\tau_{\mu_1}],\tau_{\nu_2}]\vert HF\rangle$
		$F_{\mu_2\nu_1}=(\langle \overline{t_1}\vert+\langle \overline{t_2}\vert)[[H_o,\tau_{\mu_2}],\tau_{\nu_1}]\vert HF\rangle$	$F_{\mu_2\nu_2}=\langle \overline{t_2}\vert[[H_o,\tau_{\mu_2}],\tau_{\nu_2}]\vert HF\rangle$
${}^L\eta^Y$	CCS	${}^L\eta^Y_{\nu_1}=\langle L_1\vert[\hat{Y},\tau_{\nu_1}]\vert HF\rangle$	
	CC2 & CCSD	${}^L\eta^Y_{\nu_1}=\langle L_1\vert[\hat{Y},\tau_{\nu_1}]\vert HF\rangle$ $+\langle L_2\vert[\hat{Y}+[\hat{Y},T_2],\tau_{\nu_1}]\vert HF\rangle$	${}^L\eta^Y_{\nu_2}=(\langle L_1\vert+\langle L_2\vert)[Y,\tau_{\nu_2}]\vert HF\rangle$
${}^L\mathbf{F}$	CCS	${}^LF_{\mu_1\nu_1}=\langle L_1\vert\vert[[\hat{H}_o,\tau_{\mu_1}],\tau_{\nu_1}]\vert HF\rangle$	
	CC2	${}^LF_{\mu_1\nu_1}=(\langle L_1\vert+\langle L_2\vert)[[\hat{H}_o,\tau_{\mu_1}],\tau_{\nu_1}]\vert HF\rangle$	${}^LF_{\mu_1\nu_2}=\langle L_1\vert[[H_o,\tau_{\mu_1}],\tau_{\nu_2}]\vert HF\rangle$
		${}^LF_{\mu_2\nu_1}=\langle L_1\vert[[H_o,\tau_{\mu_2}],\tau_{\nu_1}]\vert HF\rangle$	${}^LF_{\mu_2\nu_2}=0$
	CCSD	${}^LF_{\mu_1\nu_1}=(\langle L_1\vert+\langle L_2\vert)[[\hat{H}_o,\tau_{\mu_1}],\tau_{\nu_1}]\vert HF\rangle$ $+\langle L_2\vert[[[\hat{H}_o,\tau_{\mu_1}],\tau_{\nu_1}],T_2]\vert HF\rangle$	${}^LF_{\mu_1\nu_2}=(\langle L_1\vert+\langle L_2\vert)[[H_o,\tau_{\mu_1}],\tau_{\nu_2}]\vert HF\rangle$
		${}^LF_{\mu_2\nu_1}=(\langle L_1\vert+\langle L_2\vert)[[H_o,\tau_{\mu_2}],\tau_{\nu_1}]\vert HF\rangle$	${}^LF_{\mu_2\nu_2}=\langle L_2\vert[[H_o,\tau_{\mu_2}],\tau_{\nu_2}]\vert HF\rangle$

[a]See text for definitions.
[b]Equal to zero for a HF reference state.

$$T^Y_{of}=\eta^Y R^f+\overline{M^f}(\omega_f)\xi^Y, \tag{49}$$

where the $\overline{M^f}$ vector is determined from

$$\overline{M^f}(\omega_f)(\omega_f\mathbf{1}+\mathbf{A})+\mathbf{F}R^f=0. \tag{50}$$

It is advantageous to use Eq. (49) in cases where transition properties are requested for several operators Y at the same time, since only one additional equation (for $\overline{M^f}(\omega_f)$) needs to be solved for calculating all transition properties to each excited state. Equation (48) requires the solution of one additional equation for each perturbation Y.

Excited-state first-order properties can be determined from

$$\langle X\rangle^f=\sum_{pq} D^f_{pq}X_{pq} \tag{51}$$

where the excited-state one-electron density matrix is

$$\begin{aligned}D^f_{pq}=\frac{1}{2}P(p,q)\{&(\langle HF\vert+\langle \overline{t^f_1}\vert)\hat{E}_{pq}\vert HF\rangle+(\langle \overline{t^f_1}\vert+\langle \overline{t^f_2}\vert)\\ &\times[\hat{E}_{pq},T_2]\vert HF\rangle+\langle L^f_1\vert[\hat{E}_{pq},R^f_1]\vert HF\rangle\\ &+\langle L^f_2\vert[[\hat{E}_{pq},T_2],R^f_1]\vert HF\rangle+(\langle L^f_1\vert+\langle L^f_2\vert)\\ &\times[\hat{E}_{pq},R^f_2]\vert HF\rangle\}.\end{aligned} \tag{52}$$

$\hat{E}_{pq}$ is T_1-transformed E_{pq} operators as in Eq. (28). We have introduced the excited-state zero-order Lagrange multipliers $\overline{t^f}$ obtained from

$$\overline{t^f}\mathbf{A}+\eta^f=0, \tag{53}$$

where the η^f vector can be written as

$$\eta^f=\eta+L^f\mathbf{B}R^f. \tag{54}$$

The matrix **B** is defined implicitly in Eq. (59) below. Equation (52) holds for CC2 and CCSD. CCS is obtained by putting all double excitation vectors (L^f_2,R^f_2,t_2,t^f_2) to zero in Eq. (52). The ground-state result is obtained by using the ground-state $\overline{t}$ Lagrange multipliers rather than $\overline{t^f}$ and neglecting the terms containing L^f and R^f.

In coupled cluster theory, the transition strength for transition between excited states can be evaluated as

$$S^{if}_{XY}=\frac{1}{2}(T^X_{if}T^Y_{fi}+(T^Y_{if}T^X_{fi})^*), \tag{55}$$

where the transition-matrix elements can be obtained as

$$T^X_{if}=L^i\mathbf{A}^XR^f+\overline{N^{if}}(\omega_i,\omega_f)\xi^X. \tag{56}$$

The matrix $\mathbf{A^X}$ is defined implicitly in Eq. (58) below. The $\overline{N^{if}}(\omega_i,\omega_f)$ vector is obtained from

$$\overline{N^{if}}(\omega_i,\omega_f)((\omega_f-\omega_i)\mathbf{1}+\mathbf{A})+L^i\mathbf{B}R^f=0. \tag{57}$$

For calculations of transition-matrix elements between excited states and excited-state first-order molecular properties, it is convenient to use ''left''-transformed $\mathbf{A}^X$ and $\mathbf{B}$ matrices, since these are structurally closely related to the η^Y vector and the $\mathbf{F}$ matrix respectively. Accordingly, we introduce the vectors

$${}^L\eta^Y=L^f\mathbf{A}^X, \tag{58}$$

$${}^L\mathbf{F}=L^f\mathbf{B}. \tag{59}$$

Expressions for the ${}^L\eta^Y$ vector and the ${}^L\mathbf{F}$ matrix for CCS, CC2 and CCSD are given in Table I.

Excitation energies, excited-state properties, transition strengths, and second-order dynamical properties including the frequency-dependent polarizability have now been defined for CCS, CC2, and CCSD. In the next subsection, we describe their implementation in more detail.

D. Implementation of integral-direct coupled cluster linear response

Our implementation for the calculation of integral-direct coupled cluster ground-state energies,[4,5] excitation energies[6,7] and first-order one-electron ground-state properties[8] has been described previously and is incorporated in a local version of the Dalton program.[23] In this section, we describe an integral-direct implementation of coupled cluster linear-response properties, excited-state one-electron properties and transition-matrix elements between excited states.

Our present implementation is general in the sense that arbitrary Hermitian one-electron singlet operators can be treated, provided the integrals over the particular one-electron operators are available. The electric dipole–dipole and m-pole–n-pole frequency-dependent polarizabilities are therefore special cases. Specifying the one-electron operator as the electronic angular-momentum operator, we may determine the paramagnetic contribution to the magnetizability from the linear-response function and the rotational strengths from its residues. The use of perturbation-dependent basis functions such as London orbitals has not yet been implemented. At present, our implementation is restricted to (1) one-electron operators and (2) operators of singlet spin symmetry. The latter restriction has been imposed for reasons of efficiency in calculations on singlet excited states and singlet perturbation operators.

The implementation allows for the use of both forms of the linear-response function [Eqs. (36) and (39)] and for both forms of the transition strength [constructed from Eq. (46) using Eq. (47) together with either Eq. (48) or Eq. (49)]. The expressions that, in standard applications, are the most efficient [Eqs. (36) and (49)] are used as default. The present implementation is thus more flexible than the previous implementation of the frequency-dependent polarizability.[15] It also contains the $C^{\pm\omega}$ symmetrizer in Eqs. (36), (39), thereby ensuring that the linear-response function satisfies the symmetry relation Eq. (6). Similarly, the transition-strength matrix in Eq. (46) is different and more general than in the previous implementation of coupled cluster transition properties,[21] as it is based on the expression for the response function that satisfy the symmetry relations imposed by the $C^{\pm\omega}$ symmetrizer in Eqs. (36), (39). Furthermore, the use of the Lagrange-multiplier type vector $\overline{M^f}$ in Eq. (49) is computationally advantageous relative to the use of Eq. (48) that is used in Ref. 21. The expression for the excited-state property is equivalent to the non-orbital relaxed special case of the implementation in Ref. 22, with an explicit symmetrization of the one-electron density to ensure that the expectation value of an imaginary operator vanishes for non-degenerate states. The response transition-matrix elements between excited states have not previously been implemented.

The calculations of response functions and their residues are broken down into linear-algebra subtasks, thereby reducing the most difficult steps to a few well-defined tasks. As an illustration, consider the calculation of a set of linear-response properties according to Eq. (36). Assuming the Hartree–Fock state has been optimized, the procedure is as follows

(1) Determine the reference amplitudes t, Eq. (26).
(2) Determine the zero-order Lagrange multipliers $\overline{t}$, Eq. (42).
(3) Solve simultaneously all required first-order t-responses $t^Y(\omega_y)$, Eq. (38).
(4) Calculate the F-transformed vectors: $\gamma^Y(\omega_y)=\mathbf{F}t^Y(\omega_y)$.
(5) Calculate the linear response property according to Eq. (36).

Step 1 is carried out by using the direct inversion in the iterative subspace (DIIS) algorithm,[24] requiring the construction of the e vector for a set of trial amplitudes. The integral-direct construction of the e vector function Eq. (26) proceeds as in Refs. 4,5: The atomic-orbital (AO) integrals are calculated in distributions, with three free AO indices and one fixed AO index δ

$$I^{\delta}_{\alpha\beta,\gamma}=(\alpha\beta|\gamma\delta)\,\alpha\leqslant\beta. \tag{60}$$

All distributions belonging to the same shell are calculated simultaneously and written to disk. The distributions are subsequently read back into memory, one at a time, in a loop over δ belonging to the given shell. In the loop over δ, all contributions to the vector function from this particular distribution of integrals are calculated and added to the result vector.

Step 2 is carried out using iterative algorithms,[25] suitably generalized to non-symmetric matrices. This step requires the construction of linear transformations of the form

$$\sigma=b\mathbf{A}. \tag{61}$$

The integral-direct evaluation of this transformation was described in Ref. 8 for the calculation of ground-state first-order properties. The η vector is calculated from a few general intermediates stored on disk (size N^2 and $\frac{1}{2}V^2O^2$) and which are used throughout the response calculation. The η vector therefore does not require the recalculation of integrals and is computational inexpensive.

Step 3 is carried out in a similar manner, using a reduced-space iterative algorithm requiring the construction of

$$\rho = \mathbf{A}c. \tag{62}$$

An AO integral-direct implementation has been described in connection with the calculation of excitation energies.[6,7] The ξ^Y vector is calculated on the fly from one-electron integrals and t-amplitudes.

In step 4, the integral-direct F-matrix transformation of the form

$$\gamma = \mathbf{F}c \tag{63}$$

constitutes the most challenging new step. Later in this subsection, we describe how this can be accomplished using a strategy similar that in the previous steps. The η^X vector is calculated on the fly from one-electron integrals, t-amplitudes and $\overline{t}$-multipliers, and step 5 thus consists only of a few trivial dot products.

With the same basic building blocks, an efficient integral-direct calculation of transition strengths and excited-state one-electron properties can be obtained as follows:

- Solve for reference amplitudes t, Eq. (26).
- Solve for $\overline{t}$, Eq. (42).
- Solve for right eigenvectors R^f, Eq. (43).
- Solve for left eigenvectors L^f, Eq. (44).
- Construct all required η^f vectors and store on disk.
- Solve for all $\overline{t^f}$ vectors simultaneously, Eq. (53).
- Construct the excited-state one-electron density, Eq. (52).
- Calculate excited-state one-electron properties, Eq. (51).
- Construct all $\gamma^f = \mathbf{F}R^f$ vectors and store on disk.
- Solve for all $\overline{M^f}$ vectors simultaneously, Eq. (50).
- Calculate the left and right transition-matrix elements, Eqs. (49,47).
- Calculate the transition strength from Eq. (46).

The calculation of the linear-response function and transition strength in the alternative formulation is easily obtained from the same basic building blocks. The transition strength between excited state is similarly easily obtained. From the expressions in Table I, it is seen that ${}^L\eta^Y$ and η^Y and also ${}^L\mathbf{F}$ and $\mathbf{F}$ are structurally similar. The main difference is that a simple HF term is not present in ${}^L\eta^Y$ and ${}^L\mathbf{F}$ and different ''left'' amplitude are used (L instead of $\overline{t}$). The contributions from ${}^L\eta^Y$ and ${}^L\mathbf{F}$ can thus be calculated in the same way as for η^Y and $\mathbf{F}$, with a generalization to non-total symmetric ''left''-vectors.

We now discuss the F-matrix transformation in more detail for CCSD. The CCS and CC2 results can easily be obtained by skipping the appropriate terms according to the expressions in Table I. For convenience in the subsequent development, we introduce the trial-vector transformed Hamiltonian

$$\widetilde{H}_o = [\hat{H}_o, C_1] \tag{64}$$

which represents a one-index transformation of $\hat{H}_o$. The expressions for the ''right'' transformation with trial vectors of the Jacobian become

$$\rho_{\mu_1} = \langle \mu_1 | \widetilde{H}_o + [\widetilde{H}_o, T_2] + [\hat{H}_o, C_2] | HF \rangle \tag{65}$$

$$\rho_{\mu_2} = \langle \mu_2 | \widetilde{H}_o + [\widetilde{H}_o, T_2] + [\hat{H}_o, C_2] + [[H_o, C_2], T_2] | HF \rangle, \tag{66}$$

whereas the expressions for the ''left'' transformation with trial vectors of the Jacobian are given by

$$\sigma_{\nu_1} = (\langle \overline{b_1} | + \langle \overline{b_2} |)[\hat{H}_o + [\hat{H}_o, T_2], \tau_{\nu_1}] | HF \rangle, \tag{67}$$

$$\sigma_{\nu_2} = (\langle \overline{b_1} | + \langle \overline{b_2} |)[\hat{H}_o, \tau_{\nu_2}] | HF \rangle + \langle \overline{b_2} | [[H_o, T_2], \tau_{\nu_2}] | HF \rangle. \tag{68}$$

Using a similar notation, the F-matrix transformation can be expressed as

$$\gamma_{\nu_1} = \langle HF | [\widetilde{H}_o, \tau_{\nu_1}] | HF \rangle + (\langle \overline{t_1} | + \langle \overline{t_2} |)[\widetilde{H}_o + [\hat{H}_o, C_2], \tau_{\nu_1}] | HF \rangle + \langle \overline{t_2} | [[\widetilde{H}_o, T_2], \tau_{\nu_1}] | HF \rangle, \tag{69}$$

$$\gamma_{\nu_2} = (\langle \overline{t_1} | + \langle \overline{t_2} |)[\widetilde{H}_o, \tau_{\nu_2}] | HF \rangle + \langle \overline{t_2} | [[[H_o, C_2], \tau_{\nu_2}] | HF \rangle. \tag{70}$$

From these equations, it is clear that the F-matrix transformation can be carried out using a strategy closely related to that in the two linear transformations of the Jacobian. In Ref. 7, we described how intermediates with the $\widetilde{H}_o$ integrals can be constructed. In Ref. 8, we described how these intermediates (as well as additional intermediates) could be used for the construction of the σ vector in Eqs. (67), (68). From the above equations, it is seen that the terms of the F-matrix transformation reduce to terms in the ''left'' Jacobian transformation—if $\overline{t}$ is replaced by b amplitudes, and either $\widetilde{H}_o$ is replaced by $\hat{H}_o$ or C_2 is replaced by T_2. The same basic contraction routines can therefore be used in the F-matrix transformation as in the construction of the ''left'' Jacobian transformation, but the intermediates must be constructed as generalized intermediates depending on C_1 and C_2. In this way an efficient algorithm can be designed for the F-matrix transformation with essentially the same requirements as the right and left transformations. We note in passing that the F-matrix transformation contains more terms than the Jacobian transformations when the C_1 intermediates are written out as in Ref. 7.

We emphasize that, even though the F-matrix transformation does require some additional coding, the computer time spent in carrying out F-matrix transformations is small. Consider the calculation of linear-response properties. Let N_s be the number of (Y, ω_Y) sets, and N_{it} be the number of iterations typically used in solving a set of CC equations. Approximately $(2+N_s)N_{it}$ evaluations of the coupled cluster vector function or Jacobian transformations are carried out for obtaining the reference amplitudes and multipliers

TABLE II. Polarizabilities for N_2 in CCS, CC2 and CCSD for various basis sets.[a]

	CCS		CC2		CCSD	
Basis set	α_{xx}	α_{zz}	α_{xx}	α_{zz}	α_{xx}	α_{zz}
cc-pVDZ	5.961	14.505	5.848	12.422	5.797	12.756
aug-cc-pVDZ	10.165	15.682	10.091	14.400	10.003	14.610
daug-cc-pVDZ	10.424	15.811	10.258	14.524	10.192	14.740
taug-cc-pVDZ	10.435	15.814	10.269	14.530	10.203	14.745
qaug-cc-pVDZ	10.438	15.816	10.272	14.532	10.206	14.747
cc-pVTZ	7.754	15.344	7.531	13.471	7.469	13.802
aug-cc-pVTZ	10.440	15.828	10.215	14.343	10.126	14.578
daug-cc-pVTZ	10.481	15.842	10.239	14.372	10.153	14.604
taug-cc-pVTZ	10.482	15.843	10.241	14.372	10.154	14.604
qaug-cc-pVTZ	10.482	15.846	10.241	14.375	10.154	14.608
cc-pVQZ	9.016	15.646	8.734	13.897	8.679	14.218
aug-cc-pVQZ	10.480	15.826	10.189	14.285	10.108	14.541
daug-cc-pVQZ	10.481	15.831	10.193	14.296	10.109	14.548
cc-pV5Z	9.615	15.790	9.335	14.107	9.273	14.409
aug-cc-pV5Z	10.479	15.822	10.164	14.248	10.085	14.512
daug-cc-pV5Z	10.478	15.825	10.167	14.255	10.085	14.516
cc-pCVDZ	6.005	14.531	5.881	12.432	5.831	12.771
aug-cc-pCVDZ	10.161	15.695	10.066	14.393	9.978	14.604
daug-cc-pCVDZ	10.421	15.824	10.239	14.519	10.171	14.734
cc-pCVTZ	7.911	15.353	7.654	13.469	7.597	13.804
aug-cc-pCVTZ	10.441	15.825	10.185	14.314	10.098	14.556
daug-cc-pCVTZ	10.484	15.841	10.212	14.344	10.127	14.582
cc-pCVQZ	9.023	15.652	8.725	13.884	8.671	14.210
aug-cc-pCVQZ	10.481	15.826	10.169	14.266	10.089	14.526

[a]$R_{NN}=2.068$ a.u.

and the $t^Y(\omega_y)$,$(t^Y(-\omega_y))^*$ response vectors, while only N_s F-transformations are required. The fraction of computer time consumed in the F-matrix transformations for CCSD thus becomes

$$\frac{k_F N_s N^6}{k_F N_s N^6 + k_A(2+N_s)N_{it}N^6} = \frac{k_F}{k_F + k_A(2N_s^{-1}+1)N_{it}}. \tag{71}$$

Typically, N_{it} is of order 15 and k_F is less than $2k_A$. The relative amount of CPU time used in the F-matrix transformations is therefore quite small (approximately 5%–10%).

III. THE POLARIZABILITY OF N_2

The polarizability and hyperpolarizability of the nitrogen molecule have been studied extensively at different levels of theory.[26–31] We will investigate the polarizability of the nitrogen molecule using the above described coupled cluster models in the integral-direct implementation. All calculations have been carried out at the experimental bond distance of 2.068 a.u.

The polarizability calculations on the N_2 molecule were initiated by a basis-set convergence study of the static polarizability tensor. The results for the CCS, CC2, and CCSD models are given in Table II using the correlation-consistent basis sets developed by Dunning and coworkers.[32,33,26] The single most important effect comes from augmenting the cc-pVXZ (X = D, T, Q, and 5) basis sets with diffuse functions. Double augmentation of the basis set has only a small effect on the polarizability and the effect of further augmentation is marginal. The effect of the second augmentation is drastically decreased in the X = D, T, Q, 5 series. The aug-cc-pVQZ results is within a few hundreth of an a.u. of the daug-cc-pV5Z results. The CC2 and CCSD models show almost the same basis-set convergence pattern, while the CCS model converges faster than these models.

The effect of core-valence correlation on the polarizability of the nitrogen molecule is very small; see Table II. In particular, this effect is significantly smaller than the dispersion effects, as we shall see below.

For the aug-cc-pVQZ basis, the static polarizabilities at the CCS, CC2, and CCSD levels are 12.26 a.u., 11.55 a.u., and 11.59 a.u., respectively. The experimentally estimated static polarizability is 11.74 ± 0.06 a.u.,[34], so our results are a little lower than the experimental one. This is resolved by the inclusion of triples, as can be seen in Table III. The result obtained at the CCSD(T)[35] level is 11.69 a.u., which compares significantly better with experiment. Vibrational averaging has been shown to increase the polarizability by about 0.06 a.u.,[36] so we obtain a final estimate of 11.75 a.u., in perfect agreement with the experimental value.

Frequency-dependent polarizabilites were calculated at the aug-cc-pVQZ level and the dispersion curves are given in Figs. 1 and 2. We observe that the CC2 and CCSD dispersion curves are fairly close to each other, while there are larger deviations for CCS and SCF. This complies with an

TABLE III. The polarizability of N_2 for various models in the aug-cc-pVQZ basis set.[a,b]

Basis set	α_{xx}	α_{zz}	α
CCS	10.48	15.83	12.26
SCF	9.81	14.95	11.52
MP2	10.09	14.22	11.47
CC2	10.19	14.29	11.55
CCSD	10.11	14.54	11.59
CCSD(T)	10.17	14.72	11.69

[a]$R_{NN}=2.068$ a.u.
[b]The CCS, CC2 and CCSD results are calculated using the expressions given in this paper, while the MP2 and CCSD(T) results are obtained from a finite field calculation.

improved polestructure in CC2 and CCSD relative to the uncorrelated methods.

An old experimental polarizability of 11.92 a.u. at $\omega=0.07200$ exists.[37] Comparing this with the aug-cc-pVQZ CCSD static value of 11.59 a.u. and the frequency-dependent value of 11.73 a.u. at this frequency, we find a dispersion of 0.14 a.u. close to the one observed experimentally. In Fig. 3, the dispersion curve of the refractive index ($n=1+2\pi\alpha(\omega)N$, where N is the number of molecules per unit volume) is compared to different experiments.[38,39] As can be seen, the dispersion at the CC2 and CCSD levels is similar to the one observed experimentally. The CC2 and CCSD curves are a little lower than the experimental curve, which compare favorably with the result above, where CCSD(T) increased the static polarizability by 0.9% compared to CCSD.

IV. THE EXCITED STATES OF FURAN

A. Computational details

All calculations have been carried out at the experimental geometry.[40] For the molecule-centered basis functions, we have used the same center as Serrano *et al.*[41] This center was obtained as the average between the center of the charge-centroids of the $^2A_2$ and $^2B_1$ furan cations. The distance from the oxygen atom is 1.487 Å.

In Table IV, we have listed the basis sets used in this study together with the total number of basis functions and the Hartree–Fock energy. The ANO basis set of Ref. 41 was used to simplify the comparison with the CASSCF and CASPT2 results. This basis set contains an atom-centered basis set of diffuse polarized double-zeta quality and a set of $2s2p2d$ molecule-centered functions. In the basis-set investigation and the large-scale calculations, we have used basis sets constructed as extensions to the correlation-consistent cc-pVDZ and cc-pVTZ basis sets.[32] The D+ and T+ basis sets contain the diffuse basis functions of the aug-cc-pVDZ and aug-cc-pVTZ basis sets,[33] respectively, except for the diffuse function of the highest angular momentum. The D+7, D+10 and T+7 basis set contain additional molecule-centered basis functions constructed as proposed by Kaufmann *et al.*[42] The exponents are listed in Table IV. The D+7 and T+7 sets both contain the same set of molecule-centered functions—namely, the set of $7s7p7d$ functions chosen with ''semi-quantum numbers'' from 2.5 to 5.5, in half-integral steps. The D+10 basis is an extension to the D+7 basis and includes $10s10p10d$ functions with ''semi-quantum numbers'' from 2.0 to 6.5. In the coupled cluster calculations, the core electrons were frozen in the canonical Hartree–Fock orbitals as the basis set does not include any core-correlating orbitals. Core effects are expected to be at most a few hundreth of an eV.

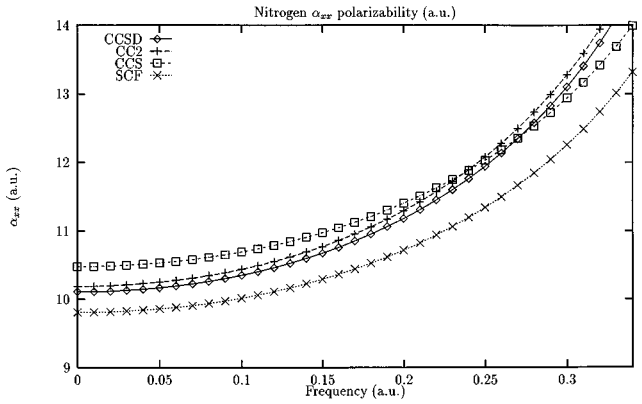

FIG. 1. The α_{xx} polarizability (in a.u.) of N_2 plotted against ω (in a.u.).

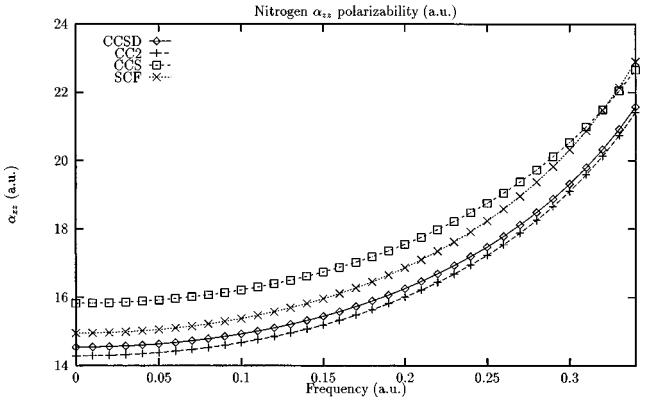

FIG. 2. The α_{zz} polarizability (in a.u.) of N_2 plotted against ω (in a.u.).

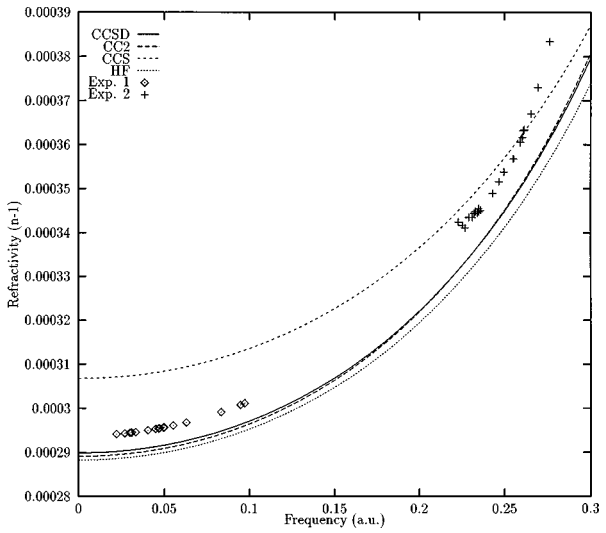

FIG. 3. Index of refraction for N_2 plotted against ω (in a.u.).

TABLE IV. Basis sets employed for furan.

Name	Standard name	Atom basis C–O	Atom basis H	Center basis	N	E_{SCF}
D	cc-pVDZ	$[3s2p1d]$	$[2s1p]$	-	90	−228.708675
aD	aug-cc-pVDZ	$[4s3p2d]$	$[3s2p]$	-	151	−228.654089
aT	aug-cc-pVTZ	$[5s4p3d2f]$	$[4s3p2d]$	-	322	−228.709338
ANO		$[4s3p1d]$	$[2s1p]$	$2s2p2d$	128	−228.703159
D+7		$[4s3p1d]$	$[3s1p]$	$7s7p7d$(2.5-5.5)	177	−228.648746
D+10		$[4s3p1d]$	$[3s1p]$	$10s10p10d$(2.0-6.5)	204	−228.649145
T+7		$[5s4p3d1f]$	$[4s3p1d]$	$7s7p7d$(2.5-5.5)	330	−228.656267
Center functions[a]		*s*	*p*	*d*		
2.0		0.024623933	0.042335280	0.060540203		
2.5		0.011253343	0.019254206	0.027445693		
3.0		0.005858381	0.009988210	0.014204399		
3.5		0.003345974	0.005689361	0.008076593		
4.0		0.002048422	0.003475680	0.004927186		
4.5		0.001323642	0.002242059	0.003174811		
5.0		0.000893096	0.001510640	0.002137123		
5.5		0.000624313	0.001054753	0.001491012		
6.0		0.000449505	0.000758656	0.001071740		
ANO $2s2p2d$ Center functions[b]		*s*	*p*	*d*		
		0.04712	0.4256	0.02850		
		0.01860	0.01680	0.01125		

[a]Constructed according to Ref. 41.
[b]From Ref. 41.

B. *N*-electron model convergence

In Tables V, VI, and VII, we give vertical excitation energies, oscillator strengths, and excited-state properties for the different coupled cluster models in the ANO basis set. From the $\%T_1$ weights in the solution vectors, we see that all excitations are primarily one-electron excitations. All have $\%T_1 \approx 95$, the only exception being the 2^1A_1 state, which has a slightly larger doubles weight. In agreement with these observations, we find small effects of triple excitations on the excitation energies. For the Rydberg states, the triples effects are of order of −0.06 eV. For the valence states, the triples effects range from −0.07 eV to −0.26 for the 2^1A_1 state. The CCSDR(3) triples correction gives excitation energies within a few hundreths of an eV from the CC3 results, and thus contains the major part of the CC3 correction. The CC2 results are within 0.3 eV of the CC3 results. Rather

TABLE V. Vertical excitation energies for furan in eV. $\%T_1$ is the percentage weight of single excitations in the CCSD right solution vectors.[a,b]

	CCS[c]	CC2	CCSD	CCSDR(3)	CC3	T_1	CAS[d]	CASPT2[d]	Assignment
$^1A_1$	8.090	6.823	6.861	6.688	6.606	91	6.74	6.16	Valence
	7.317	7.288	7.486	7.448	7.437	96	7.47	7.31	$1a_2 \rightarrow 3d_{xy}$
	8.702	7.851	8.136	8.112	8.097	95			$2b_1 \rightarrow 3p_x$
	8.953	8.387	8.559	8.399	8.349	94	10.63	7.74	Valence
$^1B_1$	6.465	6.419	6.562	6.517	6.504	96	6.22	6.46	$1a_2 \rightarrow 3p_y$
	7.162	7.059	7.240	7.193	7.180	96	6.87	7.15	$1a_2 \rightarrow 3d_{yz}$
	8.122	7.166	7.423	7.378	7.360	95	7.36	7.21	$2b_1 \rightarrow 3s$
	8.811	7.749	8.034	8.007	7.991	95			$2b_1 \rightarrow 3p_z$
$^1B_2$	6.319	6.403	6.489	6.384	6.352	95	9.10	6.04	Valence
	6.757	6.786	6.904	6.835	6.824	95	6.58	6.48	$1a_2 \rightarrow 3p_x$
	7.476	7.460	7.659	7.608	7.595	96	7.21	7.13	$1a_2 \rightarrow 3d_{xz}$
	9.479	8.465	8.806	8.785	8.769	94			$2b_1 \rightarrow 3d_{xy}$
	9.035	9.002	9.133	9.059	9.043	95			
	10.196	8.909	9.165	9.098	9.087	95		(8.38)	(Valence)
$^1A_2$	5.987	5.910	6.035	5.977	5.964	96	5.93	5.92	$1a_2 \rightarrow 3s$
	6.692	6.567	6.725	6.671	6.654	96	6.51	6.59	$1a_2 \rightarrow 3p_z$
	6.993	6.937	7.081	7.029	7.014	96	6.91	7.00	$1a_2 \rightarrow 3d_{x^2-y^2}$
	7.219	7.163	7.327	7.277	7.263	96	7.07	7.22	$1a_2 \rightarrow 3d_{z^2}$
	8.829	7.710	8.018	7.980	7.961	95			$2b_1 \rightarrow 3p_y$

[a]Basis set (ANO basis see Table IV) and geometry as in the CAS and CASPT2 study of Ref. 41.
[b]The 1*s* orbitals on C and O are frozen in the coupled cluster calculations.
[c]CCS and CIS excitation energies are identical.
[d]CAS and CASPT2 results from Ref. 41.

TABLE VI. Oscillator strengths for furan in coupled cluster calculation compared to previous results using same basis set and geometry.[a,b]

	CIS	CCS	CC2	CCSD	CAS/CASPT2[c]	Assignment
$^1A_1$	0.00102	0.00123	0.00197	0.00102	0.0015	Valence
	0.00003	0.00003	0.00000	0.00003	0.0003	$1a_2 \rightarrow 3d_{xy}$
	0.01877	0.01660	0.01757	0.02123		$2b_1 \rightarrow 3p_x$
	0.51361	0.41642	0.19378	0.34402	0.4159	Valence
$^1B_1$	0.04811	0.04576	0.03943	0.04087	0.0309	$1a_2 \rightarrow 3p_y$
	0.00016	0.00014	0.00150	0.00034	0.0000	$1a_2 \rightarrow 3d_{yz}$
	0.04685	0.04342	0.01892	0.02102	0.0192	$2b_1 \rightarrow 3s$
	0.00125	0.00105	0.00533	0.00553		$2b_1 \rightarrow 3p_z$
$^1B_2$	0.19839	0.16830	0.14935	0.14874	0.1543	Valence
	0.00602	0.00336	0.01347	0.00488	0.0471	$1a_2 \rightarrow 3p_x$
	0.01540	0.01246	0.01798	0.01297	0.0074	$1a_2 \rightarrow 3d_{xz}$
	0.00909	0.00845	0.02360	0.03564		$2b_1 \rightarrow 3d_{xy}$
	0.01323	0.01148	0.00241	0.08147		
	0.24550	0.19779	0.17065	0.04471	(0.27)	

[a]Basis set and geometry(ANO basis see Table IV) as in the CAS and CASPT2 study of Ref. 41.
[b]The 1*s* orbitals on C and O are frozen in the CIS, CCS, CC2 and CCSD calculations.
[c]CAS and CASPT2 results from Ref. 41. Transition matrix elements combined with CAS and CASPT2 energy differences.

large errors (up to 1.4 eV) persist for the CCS model. As a consequence of such large errors, CCS often gives a wrong ordering of the states. For the close-lying 5 and 6 states of $^1B_2$ symmetry, CC2 reverses the order and significant shifts are found from CC2 to CCSD. The effect of triples for these states is small as seen comparing the CCSD and CC3 results. The fast decreasing shifts in the excitation energies in each step in the hierarchy CCS, CC2, CCSD, CC3 and the large values of the $\%T_1$ diagnostic lead us to expect highly accurate values in CC3. In previous FCI calculations, we have found a reduction in the correlation error from CCSD to CC3 of approximately a factor of three (in a basis of augmented polarized double-zeta quality). This indicates that the remaining correlation error in CC3 is very small: about 0.02 eV for the Rydberg states and less than 0.1 eV for the valence states. Implicitly, this also defines the expected accuracy of the other coupled cluster models.

Next, we discuss the calculated oscillator strengths in Table VI. For comparison, we have also included the CIS results. The CIS and CCS results are of the same order of

TABLE VII. Furan ground- and excited-states dipole moments and the second electronic moment of charge perpendicular to the molecular plane.[a,b]

	Molecular dipole moments (a.u.)					Second electronic moments (a.u.)					
	CIS	CCS	CC2	CCSD	CAS[c]	CIS	CCS	CC2	CCSD	CAS[c]	Assignment
1^1A_1	0.332	0.332	0.210	0.265	0.365	24.5	24.5	24.4	24.3	24.1	Valence
$^1A_1$	0.260	0.328	0.342	0.380	0.515	27.4	27.3	25.3	25.0	24.2	Valence
	−0.156	−0.089	−0.157	−0.104	−0.095	81.8	81.0	81.2	78.8	83.3	$1a_2 \rightarrow 3d_{xy}$
	−0.424	−0.400	−0.314	−0.149		72.1	71.2	68.1	66.5		$2b_1 \rightarrow 3p_x$
	0.843	0.835	0.290	0.257	−0.146	39.7	39.3	55.9	38.0	27.0	Valence
$^1B_1$	−0.063	−0.003	−0.234	−0.172	−0.185	37.8	37.1	36.8	36.3	37.8	$1a_2 \rightarrow 3p_y$
	0.089	0.151	0.161	0.297	0.249	39.1	38.3	37.3	36.2	39.2	$1a_2 \rightarrow 3d_{yz}$
	−2.138	−2.041	−0.951	−0.628	−0.953	41.8	41.0	39.7	39.6	41.0	$2b_1 \rightarrow 3s$
	-0.596	−0.584	−0.110	−0.141		40.0	39.2	37.9	37.4		$2b_1 \rightarrow 3p_z$
$^1B_2$	1.346	1.278	1.272	1.206	0.123	38.4	38.1	44.2	39.7	30.2	Valence
	−1.751	−1.626	−2.102	−1.857	0.418	59.5	58.9	54.1	56.0	66.6	$1a_2 \rightarrow 3p_x$
	0.557	0.600	0.731	0.691	−0.564	84.1	83.4	82.3	81.4	78.9	$1a_2 \rightarrow 3d_{xz}$
	0.322	0.127	−0.142	−0.164		80.8	79.9	77.1	71.2		$2b_1 \rightarrow 3d_{xy}$
	−0.563	−0.470	−0.281	−1.086		70.3	69.6	62.1	63.1		
	0.089	0.127	−0.543	0.433		30.6	30.4	42.6	50.1		
$^1A_2$	−0.189	−0.115	−0.477	−0.384	−0.423	41.9	41.2	39.4	39.1	40.7	$1a_2 \rightarrow 3s$
	−0.787	−0.685	−0.648	−0.604	−0.490	38.7	38.0	37.2	36.7	37.9	$1a_2 \rightarrow 3p_z$
	0.025	0.067	0.208	0.234	0.108	50.5	49.8	42.9	41.8	49.0	$1a_2 \rightarrow 3d_{x^2-y^2}$
	0.528	0.583	0.263	0.568	−0.470	54.2	53.5	61.9	55.8	67.5	$1a_2 \rightarrow 3d_{z^2}$
	−1.167	−1.153	−0.443	−0.312		38.7	38.9	37.9	38.8		$2b_1 \rightarrow 3p_y$

[a]Basis set and geometry(ANO basis see Table IV) as in the CAS and CASPT2 study of Ref. 41.
[b]The 1*s* orbitals on C and O are frozen in the CIS, CCS, CC2 and CCSD calculations.
[c]CAS results from Ref. 41.

TABLE VIII. CCSD vertical excitation energies and oscillator strengths for furan in selected basis sets.[a,b,c]

	Excitation energies				Oscillator strengths				
	ANO	D+7	D+10	T+7	ANO	D+7	D+10	T+7	
$^1A_1$	6.861	6.875	6.868	6.821	0.0010	0.0003	0.0002	0.0000	Valence
	7.486	7.430	7.424	7.578	0.0000	0.0000	0.0000	0.0000	$1a_2 \rightarrow 3d_{xy}$
		8.040	8.034	8.197		0.0040	0.0069	0.0047	$1a_2 \rightarrow 4d_{xy}$
	8.136	8.102	8.093	8.256	0.0212	0.0160	0.0161	0.0453	$2b_1 \rightarrow 3p_x$
	8.559	8.407	8.387	8.337	0.3440	0.3496	0.3553	0.3551	Valence
		8.341	8.341	8.502		0.0025	0.0034	0.0002	$1a_2 \rightarrow 5d_{xy}$
		8.528	8.496	8.688		0.0004	0.0002		
$^1B_1$	6.562	6.506	6.505	6.642	0.0409	0.0350	0.0360	0.0354	$1a_2 \rightarrow 3p_y$
	7.240	7.191	7.190	7.323	0.0003	0.0007	0.0007	0.0005	$1a_2 \rightarrow 3d_{yz}$
	7.423	7.372	7.366	7.521	0.0210	0.0220	0.0227	0.0231	$2b_1 \rightarrow 3s$
		7.745	7.746	7.899		0.0035	0.0036		$1a_2 \rightarrow 4p_y$
	8.034	7.947	7.946	8.102		0.0017	0.0018		$2b_1 \rightarrow 3p_z$
		8.016	8.013	8.169		0.0024	0.0023		$1a_2 \rightarrow 4d_{yz}$
		8.186	8.187	8.340		0.0018	0.0016		$1a_2 \rightarrow 5p_y$
		8.298	8.298	8.425		0.0000	0.0000		$1a_2 \rightarrow 5d_{yz}$
		8.377	8.362			0.0012	0.0039		
$^1B_2$	6.489	6.484	6.477	6.453	0.1487	0.1436	0.1456	0.1642	Valence
	6.904	6.880	6.863	6.938	0.0049	0.0148	0.0116	0.0001	$1a_2 \rightarrow 3p_x$
	7.659	7.586	7.584	7.717	0.0130	0.0165	0.0172	0.0117	$1a_2 \rightarrow 3d_{xz}$
		7.787	7.785	7.936		0.0009	0.0015		$1a_2 \rightarrow 4p_x$
		8.104	8.104	8.257		0.0042	0.0047		$1a_2 \rightarrow 4d_{xz}$
		8.202	8.203	8.360		0.0011	0.0015		$1a_2 \rightarrow 5p_x$
		8.363	8.362	8.521		0.0019	0.0021		$1a_2 \rightarrow 5d_{xz}$
		8.416	8.416	8.576		0.0009	0.0012		
		8.549	8.507	8.707		0.0023	0.0012		
$^1A_2$	6.035	5.986	5.983	6.111					$1a_2 \rightarrow 3s$
	6.725	6.669	6.667	6.802					$1a_2 \rightarrow 3p_z$
	7.081	7.026	7.014	7.121					$1a_2 \rightarrow 3d_{x^2-y^2}$
	7.327	7.274	7.257	7.385					$1a_2 \rightarrow 3d_{z^2}$
		7.544	7.545	7.697					$1a_2 \rightarrow 4s$
		7.776	7.777	7.930					$1a_2 \rightarrow 4p_z$
		7.883	7.882	8.028					$1a_2 \rightarrow 4d_{x^2-y^2}$
		7.961	7.956	8.104					$1a_2 \rightarrow 4d_{z^2}$
	8.018	7.987	7.985	8.144					$2b_1 \rightarrow 3p_y$
		8.100	8.101	8.260					$1a_2 \rightarrow 5s$
		8.203	8.204	8.362					
		8.253	8.253	8.391					

[a]Geometry as in the CAS and CASPT2 study of Ref. 41.
[b]The 1*s* orbitals on C and O are frozen in the coupled cluster part of the calculation.
[c]Basis set is listed in Table IV and described in the text.

magnitude. The behavior in the hierarchy CCS, CC2 and CCSD is less systematic than for excitation energies. However, in most cases there is qualitatively good agreement among the models concerning the prediction of the relative strengths. For the higher excited valence state of $^1B_2$ symmetry, there is, however, substantial variations, indicating that the mixing of the valence state with the nearby Rydberg states is treated differently in the different models.

The excited-state properties are very informative for characterization of the excited states. A rather unambiguous assignment of the states is obtained from the second moments of the electronic charge distribution and considerations of the occupied orbital from which the primary excitation occurs. For three out of four valence states, the characterization based on the dipole moment and the second moment of charge for the excited state is unambiguous. For the highest valence $^1B_2$ state, there is again large oscillations. Based on the CCSD results, there is substantial mixing of this state with the Rydberg states. We note again, that the excitation energy of this state is only changed a little by the inclusion of triples, indicating the stability of the description. On the other hand, the electronic states are very close and the character of the states are very sensitive to the used model and basis. We further note, that the ANO basis set is not adequate for describing many of the states that are present in the same energy region. Finally, we note that there is very little difference between CIS and CCS, in particular compared with the large differences between CCS and the CC2 and CCSD results. The CC2 model offers a significant improvement on the CCS results.

C. Basis-set effects

In Tables VIII and IX, selected excitation energies, oscillator strengths, and excited-state properties are given for furan in the ANO, D+7, D+10, and T+7 basis sets. For the

TABLE IX. CCSD excited state properties for furan in selected basis sets.[a,b,c]

	Properties in D+7 basis				Properties in T+7 basis				
	$\langle z\rangle$	$\langle x^2\rangle$	$\langle y^2\rangle$	$\langle z^2\rangle$	$\langle z\rangle$	$\langle x^2\rangle$	$\langle y^2\rangle$	$\langle z^2\rangle$	Assignment
$^1A_1$	0.273	24.3	134.9	133.3	0.263	24.0	134.6	132.9	Valence
$^1A_1$	0.367	25.6	136.7	134.6					Valence
	−0.037	87.3	193.4	151.0					$1a_2\rightarrow 3d_{xy}$
	−0.063	215.7	313.8	193.4					$1a_2\rightarrow 4d_{xy}$
	−0.188	137.1	219.5	167.1					$2b_1\rightarrow 3p_x$
	0.147	42.2	146.4	146.2					Valence
	−0.096	660.1	765.9	341.8					$1a_2\rightarrow 5d_{xy}$
$^1B_1$	−0.145	35.9	180.4	145.5	−0.142	35.1	179.1		$1a_2\rightarrow 3p_y$
	0.574	35.9	176.7	174.8	0.694	34.9	174.4		$1a_2\rightarrow 3d_{yz}$
	−0.714	41.9	154.2	152.9	−0.651	41.0	153.0		$2b_1\rightarrow 3s$
	−0.966	92.5	340.1	201.6					$1a_2\rightarrow 4p_y$
	0.717	66.8	253.4	264.2					$2b_1\rightarrow 3p_z$
	0.784	62.6	234.6	250.8					$1a_2\rightarrow 4d_{yz}$
	−2.890	217.5	715.8	332.7					$1a_2\rightarrow 5p_y$
	4.132	201.7	669.8	653.4					$1a_2\rightarrow 5d_{yz}$
$^1B_2$	1.264	43.7	141.1	137.7	0.950	33.6	138.3	135.6	Valence
	−1.997	60.9	141.3	149.1	−1.539	65.2	142.5	147.9	$1a_2\rightarrow 3p_x$
	2.371	105.5	155.3	204.9	1.784	99.8	153.1	201.9	$1a_2\rightarrow 3d_{xz}$
	−2.705	239.5	200.0	208.2					$1a_2\rightarrow 4p_x$
	3.163	309.8	223.3	405.8					$1a_2\rightarrow 4d_{xz}$
	−3.696	636.5	332.2	344.1					$1a_2\rightarrow 5p_x$
	4.431	716.5	358.8	804.3					$1a_2\rightarrow 5d_{xz}$
$^1A_2$	−0.356	40.8	151.2	149.6					$1a_2\rightarrow 3s$
	−0.471	37.7	148.1	181.9					$1a_2\rightarrow 3p_z$
	0.469	39.9	177.5	143.4					$1a_2\rightarrow 3d_{x^2-y^2}$
	0.829	51.0	144.7	189.2					$1a_2\rightarrow 3d_{z^2}$
	−0.806	135.2	206.0	209.5					$1a_2\rightarrow 4s$
	−0.775	97.4	201.9	353.6					$1a_2\rightarrow 4p_z$
	−0.261	110.1	337.1	185.3					$1a_2\rightarrow 4d_{x^2-y^2}$
	1.055	126.7	191.7	354.6					$1a_2\rightarrow 4d_{z^2}$
	0.098	71.4	237.7	182.0					$2b_1\rightarrow 3p_y$
	−0.643	383.3	308.2	374.7					$1a_2\rightarrow 5s$

[a]Geometry as in the CAS and CASPT2 study of Ref. 41.
[b]The 1*s* orbitals on C and O are frozen in the coupled cluster part of the calculation.
[c]Basis set is listed in Table IV and described in the text.

excitation energies, we note that the changes from the D+7 to D+10 basis set are very small—typically less than 0.01 eV. With the $7s7p7d$ molecule-centered basis functions, we are thus close to saturation with respect to these functions. For the valence states, the effect of going from D+7 to T+7 is also rather small. The largest change is 0.07 eV, which is for the highest of the valence states of $^1A_1$ symmetry. The ANO basis result is 0.22 eV higher than the T+7 results. For the Rydberg states, the effect is somewhat larger going from D+7 to T+7. The shifts from D+7 to T+7 are practically the same for nearly all Rydberg states, around +0.15 eV.

The oscillator strengths for the intense valence states are similar for all the considered basis set. For the Rydberg states, some changes occur from ANO to D+7, whereas the results obtained for the D+7 and D+10 basis sets are very similar. It thus appears that, at the D+7 level, saturation with respect to the molecule-centered functions has been reached for the reported Rydberg states. Sample calculations are presented for the T+7 basis set. Very small relative changes have been obtained for the valence excitations that have large oscillator strengths going from the D+7 to T+7 basis. However for the close-lying Rydberg states large relative changes occur in the oscillator strengths. For example the oscillator strengths for the $2b_1\rightarrow 3p_x$ excitation is increased by about a factor 3 to 0.045. For the $1a_2\rightarrow 3p_x$ Rydberg excitation the oscillator strength decrease by about two orders of magnitude and nearly vanish. All reported excitations of $^1B_1$ symmetry have Rydberg character and only small changes have been obtained going from the D+7 to T+7 basis.

From Table IX, we see that the dipole moments of the excited valence states all have the same sign as that of the ground state. For the Rydberg states, this is not so and the variations of the dipole moments are considerably larger for the Rydberg states than for the valence states. Both positive and negative values occur and the states of $^1B_2$ symmetry in particular have large dipole moments compared with the ground state. For the second moment of charge, we note that, for the majority of the excited states, the x^2 component is smaller than the other two components, as the YZ plane corresponds to the molecular plane. We also see that, as expected, the second moment of charge is always larger for the

TABLE X. Previous calculated excitation energies for furan.

	MRCI[a]	SAC-CI[b]	CAS[c]	CASPT2[c]	MRCI[d]	CAS[e]	MRMP[e]	MRQD[e]	Assignment
$^1A_1$	6.79	7.32	6.74	6.16	6.02	7.09	6.16	6.19	Valence
		7.59	7.47	7.31	7.750	7.34	7.26	7.29	$1a_2\rightarrow 3d_{xy}$
		8.27			8.148				$2b_1\rightarrow 3p_x$
			10.63	7.74	8.32	10.51	7.69	7.72	Valence
					8.327				$2b_1\rightarrow 3d_{xz}$
					8.581				$1a_2\rightarrow 4d_{xy}$
$^1B_1$	6.52	6.74	6.22	6.46	6.633	6.10	6.40	6.40	$1a_2\rightarrow 3p_y$
		7.62	6.87	7.15	6.988	6.71	7.10	7.12	$1a_2\rightarrow 3d_{yz}$
	7.27	8.24	7.36	7.21	7.143	6.81	7.31	7.25	$2b_1\rightarrow 3s$
					7.652				$1a_2\rightarrow 4p_y$
					8.040				$2b_1\rightarrow 3p_z$
					8.065				$1a_2\rightarrow 4d_{yz}$
					8.359				$2b_1\rightarrow 3d_{x^2-y^2}$
					8.395				$2b_1\rightarrow 3d_{z^2}$
$^1B_2$	7.58	6.80	9.10	6.04	6.76	8.52	5.95	5.99	Valence
	6.52	7.50	6.58	6.48	6.659	6.42	6.50	6.51	$1a_2\rightarrow 3p_x$
		8.91	7.21	7.13	7.712	7.05	7.18	7.21	$1a_2\rightarrow 3d_{xz}$
					7.824				$1a_2\rightarrow 4p_x$
					8.891				$1a_2\rightarrow 4d_{xz}$
	8.60				8.936				$2b_1\rightarrow 3d_{xy}$
				8.38[f]	9.422				Valence
$^1A_2$	5.94	6.27	5.93	5.92	5.950	5.67	5.84	5.84	$1a_2\rightarrow 3s$
		6.98	6.51	6.59	6.410	6.20	6.53	6.54	$1a_2\rightarrow 3p_z$
			6.91	7.00	7.148	6.64	6.98	6.98	$1a_2\rightarrow 3d_{x^2-y^2}$
			7.07	7.22	7.405	6.77	7.18	7.19	$1a_2\rightarrow 3d_{z^2}$
					7.563				$1a_2\rightarrow 4d_{z^2}$
					7.594				$1a_2\rightarrow 4s$
					7.829				$1a_2\rightarrow 4d_{x^2-y^2}$
	7.85	8.19			7.901				$2b_1\rightarrow 3p_y$
					7.999				$2b_1\rightarrow 3d_{yz}$
					8.495				$1a_2\rightarrow 4p_z$

[a]MRCI results from Ref. 46. A range of 6.79–7.08 eV was given for the 2^1A_1 state.
[b]SAC-CI results from Ref. 44.
[c]CAS and CASPT2 results from Ref. 41.
[d]MRCI results from Ref. 45. Valence excitation energies from DZP basis set calculation. Rydberg states from DZPR basis set calculation. Other results are 6.63 eV and 9.36 eV for the $^1A_1$ valence states and 6.88 eV for the 1^1B_2.
[e]CAS,MRMP, and MRQD results from Ref. 43.
[f]Given in the text in Ref. 41.

excited state than for the ground state. For the Rydberg states we find generally increasing values for the second moment of charge with increasing quantum number as should be expected. The distribution pattern among the components relative to the ground state is seen to allow a qualitative assignment in most cases. In some cases there are mixings between the states. This, however, is not a problem for the calcultion of energies and properties, only for the qualitative interpretation. As expected the excited state dipole moments and second electronic moments are somewhat sensitive to the choice of basis set. Quite large changes occur going from the ANO basis to the D+7 basis. The sample calculations using the T+7 basis set shows up to 25% changes relative to the D+7 basis set. However qualitative the same picture is obtained in both basis sets.

D. Comparison with previous excited-state studies of furan

In Table X, we have summarized the excitation energies of previous calculations on furan. For the coupled cluster calculations in Tables V,VI and VII, we have used the same basis set and geometry as in the CASSCF and CASPT2 calculations.[41] We note that the symmetry classes B_1 and A_2 contain Rydberg states only and that the symmetry classes A_1 and B_2, in addition to Rydberg states, contain two valence states each. For the states in symmetry classes B_1 and A_2, we observe excellent agreement between the CC results and the CASPT2 results: The CASPT2 results are 0.01-0.06 eV lower than the CC3 results for the $1a_2\rightarrow 3l$ transitions, whereas a slightly larger error is observed for the $2b_1\rightarrow 3s$ transition. In view of the second-order nature of the CASPT2 approach, this accuracy is remarkably good. The picture is somewhat different for the states of symmetry A_1 and B_2, however.

First, we note that the disagreement between CC3 and CASPT2 is rather large for the valence states. The 1^1B_2 state is predicted to be about 0.3 eV higher in the CC3 calculations than in the CASPT2 calculations. However, the CASSCF result is in error by as much as 3 eV and the second-order CASPT2 correction thus does a very good job of correcting for this error. For the 2^1A_1 state, the CASPT2 result is about 0.4 eV lower than the CC3 result and the

CASSCF results are in fact more in line with the CC results.

The disagreement between the CASPT2 and CC3 results is larger for the higher valence states. The state denoted by 4^1A_1 by Serrano *et al.*, which is of valence type with a very large oscillator strength, is not found to be the fourth state but instead the fifth state in the coupled cluster calculation (recall the same ANO basis is used in the two sets of calculations). In the more complete basis set, we find even more Rydberg states entering below this state. The CASPT2 results are 0.6 eV lower than the CC3 results. The second lowest valence state of $^1B_2$ symmetry was found in the CASPT2 study at 8.38 eV, with an oscillator strength of 0.27. A state of such intensity is not found in the CC calculations below 9 eV. In this case, there is thus a discrepancy between the CC3 results and the CASPT2 results of more than 0.6 eV. It is also noteworthy that, while we in the $^1A_2$ and $^1B_1$ symmetry classes found excellent agreement for the Rydberg states in CC and CASPT2, this is not the case for these symmetry classes. The two Rydberg states of $^1B_2$ symmetry are about 0.4 eV lower in CASPT2 compared with CC3, the CASSCF results are in better agreement with CC3.

It is also interesting to compare the CC and CASSCF excited-state properties; see Table VII. First, we note that the CC and CASSCF ground-state dipole moments differ by approximately 0.1 a.u., whereas the second electronic moments are very close. The comparison for many of the other excited states reveals a similar good agreement. The most striking exceptions are the 4^1A_2 state, and the $^1B_2$ symmetry states, where very large differences exist for the dipole moments. In particular, the dipole moments of the $^1B_2$ states are qualitatively completely different in the CC and CASSCF calculations.

For the $^1A_1$ and $^1B_2$ states, we thus find a clear discrepancy in the predicted spectra of the CC and CASPT2 methods, wherease we have excellent agreement for the states in the $^1A_2$ and $^1B_1$ classes. It is relevant to emphasize, that the CC models used in this study are all ''blackbox'' approaches. The analysis of the solution vectors gives similar large $\%T_1$-diagnostics for all states and all states of all symmetries should therefore be obtained with similar high accuracy. The origin of the discrepancies between CCSD and CASPT2 are thus expected to be found in the CASPT2 calculations. This conjecture is substantiated by considering the CASPT2 calculations of Serrano *et al.*[41] In these calculations, the $^1A_1$ and $^1B_2$ states are treated with one active space, whereas the states of $^1A_2$ and $^1B_1$ symmetry are described by another. The calculations in the symmetry classes $^1A_1$ and $^1B_2$ exhibited several problems, as expressed by Serrano *et al.* The $^1A_1^+$ and $^1B_2^+$ states were placed very high in the CASSCF spectrum and a rather extensive set of states must be included in order to ''catch'' the right state in the CAS calculation. Furthermore, intruder states appeared and caused problems, in particular for the $^1A_1$ states. Therefore, the computed CASPT2 excitation energy was expected to have an uncertainty of 0.2 eV. We also note that Serrano *et al.* used a combination of state-averaged techniques and independently optimized states. For example, the 1^1A_1 state were independent optimized, whereas for the 2^1A_1 state both independently optimization and state-average techniques were used. Serrano *et al.* found little effect on this for the calculated 2^1A_1 excitation energy, indicating that state-averaged and state-specific CASPT2 calculations contain errors of the same size. We find the shift to lower excitation energies for the remaining $^1A_1$ and $^1B_2$ states striking and suggest that the uncertainty estimate for the CASPT2 calculations may be too low.

The other previous calculations were carried out using other basis sets and in some cases different ground-state geometries, making the comparison more difficult. The MRMP and MRQD results[43] are quite similar to the CASPT2 results, which is not surprising since these methods are somewhat related and the used basis sets are of similar quality. The SAC-CI approach gives somewhat different results,[44] probably because of the use of different basis sets. It is also interesting to compare with the most recent MRCI calculations, as the MRCI study, like ours, comprises a large number of states. We note that there are significant differences relative to the CC results. In the MRCI calculations, for example, the lowest Rydberg state of B_1 symmetry is found to be very close to the lowest Rydberg state of B_2 symmetry, whereas in CC we find a much larger difference. There is also disagreement in the ordering of the two lowest excited valence states, and significant numerical difference. The position of the higher excited valence states are, however, in better agreement with our results than the CASPT2 results.

V. SUMMARY

We have described an integral direct implementation of second-order frequency-dependent molecular ground state properties, one-photon transition matrix elements and excited-state one-electron properties for CCS, CC2 and CCSD. In doing so we have significantly extended the range of molecules and molecular properties that can be treated reliable in coupled cluster theory. The calculation of the abovementioned molecular properties can be divided into subunits, that all can be carried out in an integral-direct fashion. Most of them can be obtained relatively easily from our previous implementation of integral-direct techniques for the calculation of ground state energies,[4,5] excitation energies[6,7] and ground-state first-order properties.[8] The subunit that is new and common to the above mentioned properties is the contraction of the socalled F matrix on a trial vector. We have shown that this can be performed at a cost comparable to the one of a contraction of the Jacobian on a trial vector. Since the contraction of the **F** matrix with a trial vector is done once at the end of each calculation this contraction becomes a small fraction of the total calculation.

Sample calculations have been presented for the frequency-dependent polarizability of N_2 and excited-state one-electron properties and transition-properties of furan using large basis sets. The N_2 polarizability compares favorably with experiment. The furan excited-state results have been used as a benchmark in a critical comparison with other recent theoretical calculations of vertical excitation energies. In a subsequent publication the vertical excitation energy results from this paper will be combined with theoretical investigations of the excited state surfaces for a more detailed comparison with experiment.

ACKNOWLEDGMENT

This work has been supported by the Danish Natural Science Research Council (Grant No. 9600856).

[1] G. D. Purvis and R. J. Bartlett, J. Chem. Phys. **76**, 1910 (1982).
[2] R. J. Bartlett, p. 1047 in *Modern Electronic Structure Theory*, Vol. 2, edited by D. R. Yarkony (World Scientific, Singapore, 1995).
[3] P. R. Taylor, ''Accurate calculations and calibration,'' in *Lecture Notes in Quantum Chemistry, European Summer School in Quantum Chemistry*, edited by B. O. Roos (Springer-Verlag, New York, 1992); P. R. Taylor, ''Coupled cluster methods in quantum chemistry,'' in *Lecture Notes in Quantum Chemistry II, European Summer School in Quantum Chemistry*, edited by B. O. Roos (Springer-Verlag, New York, 1994).
[4] H. Koch, O. Christiansen, R. Kobayashi, P. Jørgensen, and T. Helgaker, Chem. Phys. Lett. **228**, 233 (1994).
[5] H. Koch, A. Sanchez de Meras, T. Helgaker, and O. Christiansen, J. Chem. Phys. **104**, 4157 (1996).
[6] O. Christiansen, H. Koch, P. Jørgensen, and T. Helgaker, Chem. Phys. Lett. **263**, 530 (1996).
[7] O. Christiansen, H. Koch, A. Halkier, P. Jørgensen, T. Helgaker, and A. Sanchez de Meras, J. Chem. Phys. **105**, 6921 (1996).
[8] A. Halkier, H. Koch, O. Christiansen, P. Jørgensen, and T. Helgaker, J. Chem. Phys. **107**, 849 (1997).
[9] O. Christiansen, H. Koch, and P. Jørgensen, Chem. Phys. Lett. **243**, 409 (1995).
[10] H. Koch, O. Christiansen, P. Jørgensen, A. Sanchez de Meras, and T. Helgaker, J. Chem. Phys. **106**, 1808 (1997).
[11] O. Christiansen, H. Koch, and P. Jørgensen, J. Chem. Phys. **103**, 7429 (1995).
[12] O. Christiansen, H. Koch, and P. Jørgensen, J. Chem. Phys. **105**, 1451 (1996).
[13] H. Koch, O. Christiansen, P. Jørgensen, and J. Olsen Chem. Phys. Lett. **244**, 75 (1994).
[14] O. Christiansen, H. Koch, P. Jørgensen, and J. Olsen Chem. Phys. Lett. **256**, 185 (1996).
[15] R. Kobayashi, H. Koch, and P. Jørgensen, Chem. Phys. Lett. **219**, 30 (1994).
[16] J. Gauss and J. F. Stanton, J. Chem. Phys. **103**, 3561 (1995).
[17] B. Datta, P. Sen, and D. Mukherjee, J. Phys. Chem. **99**, 6441 (1995).
[18] A. E. Kondo, P. Piecuch, and J. Paldus, J. Chem. Phys. **104**, 8566 (1996).
[19] O. Christiansen, J. Gauss, and J. F. Stanton, Chem. Phys. Lett. **266**, 53 (1997).
[20] O. Christiansen, P. Jørgensen, and C. Hättig, Int. J. Quantum. Chem. (to be published).
[21] H. Koch, R. Kobayashi, A. Sanchez de Meras, and P. Jørgensen, J. Chem. Phys. **100**, 4393 (1994).
[22] J. F. Stanton and J. Gauss, Theor. Chim. Acta **91**, 267 (1995).
[23] An electronic structure program, Release 1.0 (1997) written by T. Helgaker, H. J. Aa. Jensen, P. Jørgensen, J. Olsen, K. Ruud, H. Ågren, T. Andersen, K. L. Bak, V. Bakken, O. Christiansen, P. Dahle, E. K. Dalskov, T. Enevoldsen, B. Fernandez, H. Heiberg, H. Hettema, D. Jonsson, S. Kirpekar, R. Kobayashi, H. Koch, K. V. Mikkelsen, P. Norman, M. J. Packer, T. Saue, P. R. Taylor, and O. Vahtras.
[24] P. Pulay, Chem. Phys. Lett. **73**, 393 (1980).
[25] E. R. Davidson, J. Comput. Phys. **17**, 87 (1975); J. Phys. A **13**, L179 (1980).
[26] D. E. Woon and T. H. Dunning, J. Chem. Phys. **100**, 2975 (1994).
[27] C. Hättig and B. A. Hess, J. Chem. Phys. **105**, 9948 (1996).
[28] H. Hettema, P. E. S. Wormer, and A. J. Thakkar, Mol. Phys. **80**, 533 (1993).
[29] G. Maroulis and A. J. Thakkar, J. Chem. Phys. **88**, 7623 (1988).
[30] H. J. Aa. Jensen, P. Jørgensen, T. Helgaker, and J. Olsen, Chem. Phys. Lett. **162**, 355 (1989).
[31] H. Sekino and R. J. Bartlett, J. Chem. Phys. **98**, 3022 (1993).
[32] T. H. Dunning, J. Chem. Phys. **90**, 1007 (1989).
[33] R. A. Kendall, T. H. Dunning, and R. J. Harrison, J. Chem. Phys. **96**, 6769 (1992).
[34] G. R. Alms, A. W. Burham, and W. H. Flygare, J. Chem. Phys. **63**, 3321 (1975).
[35] K. Raghavachari, G. W. Trucks, J. A. Pople, and H. Head-Gordon, Chem. Phys. Lett. **157**, 479 (1989).
[36] D. Bishop, Rev. Mod. Phys. **62**, 343 (1990).
[37] E. W. Washburn, Ed., *International Critical Tables*, Vol. 7 (McGraw-Hill, New York, 1930).
[38] E. R. Peck and B. N. Khanna, J. Opt. Soc. Am. **56**, 1059 (1966).
[39] P. G. Wilkinson, J. Opt. Soc. Am. **50**, 1002 (1960).
[40] F. Mata, M. C. Martin, and G. O. Sørensen, J. Mol. Struct. **48**, 157 (1978).
[41] L. Serrano-Andres, M. Merchan, I. Nebot-Gil, B. O. Roos, and M. Fulscher, J. Am. Chem. Soc. **115**, 6184 (1993).
[42] K. Kaufmann, W. Baumeister, and M. Jungen, J. Phys. B: At. Mol. Opt. Phys. **22**, 2223 (1989).
[43] H. Nakano, T. Tsuneda, T. Hashimoto, and K. Hirao, J. Chem. Phys. **104**, 2312 (1996).
[44] H. Nakatsuji, O. Kitao, and T. Yonezawa, J. Chem. Phys. **83**, 723 (1985).
[45] M. H. Palmer, I. C. Walker, C. C. Ballard, and M. F. Guest, Chem. Phys. **192**, 111 (1995).
[46] K. H. Thuneman, R. J. Buenker, and W. Butscher, Chem. Phys. **47**, 313 (1980).